JOURNAL OF COMPUTATIONAL PHYSICS **127,** 316–329 (1996)
ARTICLE NO. 0178

A Piecewise-Quintic Interpolation Scheme

PIOTR HOLNICKI

Systems Research Institute, Polish Academy of Sciences, 01-447 Warsaw, ul. Newelska 6, Poland

Received June 5, 1995; revised December 5, 1995

In the paper a piecewise quintic polynomial interpolation scheme, based on a four-point stencil and a uniform grid is investigated. The interpolant utilizes four consecutive grid data points and the first derivative estimates at the internal points. Sufficient conditions for the scheme to be positive definite are formulated in terms of the discrete maximum principle. Monotonicity conditions are characterized as admissible variability regions of the respective scheme's parameters. Standard limiter functions for derivative estimates are applied with accuracy gain obtained by relaxing monotonicity constraints near local extrema. Results of numerical tests are presented for regular function interpolation as well as for 1D and 2D advection of standard test profiles. © 1996 Academic Press, Inc.

1. INTRODUCTION

Shape-preserving interpolation algorithms are now widely investigated in connection with important physical applications, for example, those related to numerical weather prediction, analysis of global climate changes, or modeling atmospheric transport processes. Used in most cases, effective semi-Lagrangian methods that follow wind characteristics backward in time require interpolation of the initial profile at the upstream departure point. It is then desired that the algorithm applied correctly reflects physical reality suggested by the data. A typical demand is, therefore, that the interpolation scheme, except the accuracy and low numerical diffusivity, should be positive definite and generate a monotone interpolant in regions where the data are monotone. In some applications, also, convexity (concavity) and conservation properties are important.

The commonly used piecewise polynomial interpolants, usually based on Hermite cubics [4–7, 10] or quintics [4, 5], give a compromise between the accuracy and computational effort, but they do not automatically preserve the shape of the data, especially on steep gradient regions or in the vicinity of local extrema. The desired positivity- or monotonicity-preserving properties are usually obtained by imposing the respective constraints on derivatives (following from sufficient conditions for the interpolation polynomial to be nonnegative/monotone) or by utilizing the limiter function that generates shape preserving derivative estimates [5–7, 10].

The major problem related to those monotonicity preserving techniques is a loss of accuracy in the vicinity of strict local extrema. The ''clipping'' effect observed results from the property that the algorithm still produces a monotone interpolant, even if the data are no longer monotone. In [10] a class of accurate, piecewise cubic schemes is considered, where the gain of the overall precision is obtained by replacing standard monotonicity conditions by high order derivative estimates in the neighborhood of local extrema. The additional mesh points must be utilized in that case to compute these estimates. This approach is also utilized in the work presented and [10] will be referred to frequently in the following.

In the paper a piecewise-quintic interpolation scheme, previously defined in [8] for the advection problem, is substantially developed, and a complex shape-preserving analysis, as well as new numerical results, are presented. The scheme considered is based on a four-point grid stencil, defined on a uniform mesh. Four consecutive grid values and the first derivative estimates at the internal points are used to construct a quintic interpolation polynomial (compare [8] for details). The interpolant is sixth-order accurate if the derivative at the grid points are of fifth order at least. It can also be combined with any algorithm of the derivative estimation, but accuracy degenerates then according to the monotonicity constraints applied. The aim of the paper is to characterize the shape-preserving properties of the scheme and to illustrate them by the respective numerical results that can be compared with other methods.

The sufficient conditions for the scheme to be positive definite are formulated in Section 3, using the discrete maximum principle approach. The results obtained are slightly stronger than the respective formulations in [8]. In Section 4 the technique applied in [10] for Hermite cubics is developed to investigate monotonicity conditions. They are formulated in terms of monotonicity regions of the respective scheme's parameters (compare also [4, 5]). Implementation of the algorithm is presented in Section 5. The interpolant is combined with some standard limiter functions for computing derivative estimates (Akima, Fritsch and Butland, ''Superbee''). To avoid accuracy degeneration by the ''clipping'' effect, parabolic approximation [10] of derivatives in

0021-9991/96 $18.00

the vicinity of extremum points is applied. Results of the numerical tests presented in Section 6 confirm good accuracy and shape preserving properties of the method. They refer to the interpolation of the exponential "bell" function [10] as well as to the application of the algorithm for 1D and 2D advection of standard test profiles.

2. INTERPOLATION POLYNOMIAL. NOTATION

Let us consider a regular grid $\{x_i\}_{i=0}^{n+2}$ for $x_0 < x_1 < \cdots < x_{n+2}$, with the mesh spacing $h = x_{i+1} - x_i$ and the corresponding data points $\{f_i\}$, which are samples of a piecewise smooth function f, such that $f_i = f(x_i)$. The slope of the piecewise linear interpolant (the first divided difference) will be denoted by

$$\Delta_i = (f_{i+1} - f_i)/h.$$

The respective set of derivative estimates at the interpolation points will be denoted by $\{d_i\}$.

To construct an interpolation polynomial in the subinterval $[x_i, x_{i+1}]$ we shall consider a four-point stencil, based on the consecutive data values f_{i-1}, f_i, f_{i+1}, f_{i+2} and the derivative estimates at the internal points, d_i, d_{i+1}. Our goal is to construct a piecewise quintic interpolation polynomial $p(x)$, such that

$$\begin{aligned} &p(x_{i+j}) = f_{i+j} \quad \text{for } i = 1, ..., n; j = -1, ..., 2, \\ &\frac{dp}{dx}(x_i) = d_i \quad \text{for } i = 1, ..., n. \end{aligned} \tag{2.1}$$

Without loss of generality, we can assume a unit length of the interpolation subinterval $-$ $[0, 1]$, corresponding to linear transformation of the independent variable $\alpha = (x - x_i)/h$, where $x \in [x_i, x_{i+1}]$. Then, as it was derived in [8], the respective interpolation polynomial has a form

$$\begin{aligned} p_i(\alpha) = c_{i-1}f_{i-1} + c_i f_i + c_{i+1}f_{i+1} + c_{i+2}f_{i+2} \\ + c_i' d_i + c_{i+1}' d_{i+1} \quad (i = 1, ..., n), \end{aligned} \tag{2.2}$$

where for $\alpha \in [0, 1]$ the coefficients are defined as

$$\begin{aligned} c_{i-1} &= \tfrac{1}{12}\alpha^2(1-\alpha)^2(2-\alpha), \\ c_i &= 1 - \alpha^2[1 + (1-\alpha^2)(\tfrac{7}{4} - \tfrac{3}{4}\alpha)], \\ c_{i+1} &= \tfrac{1}{4}\alpha^2(1+\alpha)[2 + (1-\alpha)(8-3\alpha)], \\ c_{i+2} &= \tfrac{1}{12}\alpha^2(1-\alpha^2)(1-\alpha), \\ c_i' &= \tfrac{1}{2}\alpha(1+\alpha)(1-\alpha)^2(2-\alpha), \\ c_{i+1}' &= -\tfrac{1}{2}\alpha^2(1-\alpha^2)(2-\alpha). \end{aligned} \tag{2.3}$$

It can be easily verified that for all $i = 1, ..., n$,

$$\sum_{l=-1}^{2} c_{i+l} = 1 \tag{2.4}$$

and the interpolant (2.2) satisfies the general conditions (2.1). Polynomial $p(x)$ is sixth-order accurate if the derivatives $\{d_i\}$ are fifth order at least.

In most applications the derivatives used in the interpolation scheme must be numerically approximated. The shape-preserving properties (nonnegativity, monotonicity, convexity) of the interpolant depend then essentially on the estimation method applied. The approach is usually based on the constraint that estimates (straightforward or by a limiter function) meet sufficient conditions of nonnegativity or monotonicity [4–10, 17]. Most of the algorithms utilized in the literature can be characterized as

$$d_i = G(\Delta_{i-1}, \Delta_i), \quad i = 1, ..., n, \tag{2.5}$$

where $G(s, t)$ is a nonlinear limiter function. It is commonly assumed [6, 7, 10] that G satisfies the following conditions:

$$G \text{ is symmetric, i.e., } G(s,t) = G(t,s), \tag{2.6a}$$

$$\min(|s|, |t|) \le G(s,t) \le \max(|s|, |t|), \tag{2.6b}$$

$$G \text{ is continuous}, \tag{2.6c}$$

$$G(s,t) \in I[0, \varrho \cdot \operatorname{minmod}(s,t)], \tag{2.6d}$$

where $\varrho > 0$ is a given constant. We follow here the notation applied in [10], where $I[z_1, z_2]$ denotes the smallest closed interval containing z_1, z_2; i.e.,

$$I[z_1, z_2] = [\min(z_1, z_2), \max(z_1, z_2)] \tag{2.7}$$

and

$$\operatorname{minmod}(z_1, z_2) = \begin{cases} \operatorname{sgn}(z_1) \cdot \min(|z_1|, |z_2|), & \text{if } z_1 z_2 > 0, \\ 0, & \text{if } z_1 z_2 \le 0. \end{cases} \tag{2.8}$$

To preserve monotonicity of the interpolant p_i in the case of data constant in $[x_i, x_{i+1}]$, an additional condition is imposed,

$$p_i(\alpha) = f_i \quad \text{for } [f_i = f_{i+1}] \wedge [d_i = d_{i+1} = 0]. \tag{2.6e}$$

Otherwise, the terms depending on f_{i-1} and f_{i+2} in (2.2) can violate the monotonicity in some cases (for example, if $f_i = f_{i+1} = 0$ and $f_{i-1} \neq 0$).

3. NONNEGATIVITY CONDITIONS

Positivity (nonnegativity) of the interpolation scheme is one of the essential demands considered in most applications. Violation of this condition can lead to nonphysical, negative values of the solution, overshooting the local maxima, or to spurious oscillations, especially in the vicinity of a steep gradient. If the data represent, for example, the pressure or density of material (e.g., in computational weather prediction or in modeling atmospheric pollution transport)—the negative or oscillatory values are not acceptable.

To formulate nonnegativity conditions for (2.2) note, first, that the coefficients (2.3) satisfy the following inequalities for any $\alpha \in [0, 1]$:

$$\begin{aligned} c_{i-1}(\alpha), c_i(\alpha), c_{i+1}(\alpha), c_{i+2}(\alpha) &\geq 0, \\ c_i'(\alpha) &\geq 0, \\ c_{i+1}'(\alpha) &\leq 0. \end{aligned} \tag{3.1}$$

Moreover, it can be verified by elementary calculations that

$$\begin{aligned} c_{i+1} + 2c_{i+2} + \tfrac{8}{3} c_{i+1}' &= \tfrac{1}{12} \alpha^3(11 + 6\alpha - 5\alpha^2) \geq 0, \\ 2c_{i-1} + c_i - \tfrac{8}{3} c_i' &= \tfrac{1}{12} (1 - \alpha)^3(12 + 4\alpha - 5\alpha^2) \geq 0, \end{aligned} \tag{3.2}$$

$$c_i + c_{i+1} - 3.5(c_i' - c_{i+1}') = \tfrac{1}{2} (2\alpha - 1)^2(2 + \alpha - \alpha^2) \geq 0, \tag{3.3}$$

$$\begin{aligned} c_{i+1} + 2c_{i+2} + 3.5c_{i+1}' &= \tfrac{1}{6} \alpha^2(-5 + 8\alpha + 8\alpha^2 - 5\alpha^3) > -0.0305, \\ 2c_{i-1} + c_i - 3.5c_i' &= \tfrac{1}{6} (\alpha - 1)^2(6 - 9\alpha - 7\alpha^2 + 5\alpha^3) > -0.0305. \end{aligned} \tag{3.4}$$

Now, the sufficient conditions of nonnegativity of the interpolation scheme (2.2) can be formulated in terms of the discrete maximum principle. The following two corollaries are the stronger version of the respective results presented in [8].

PROPOSITION 3.1. *Consider interpolant* (2.2) *with the coefficients defined by* (2.3). *If the limiter constant in* (2.6d) *is* $\varrho = \frac{8}{3}$ *then the piecewise quintic interpolation function* $p(x)$ *satisfies the following maximum principle* (*we denote* $p_i = p_i(\alpha)$, *for* $i = 1 \ldots n$, $\alpha \in [0, 1]$):

$$\min_{0 \leq j \leq n+2} f_j \leq p_i \leq \max_{0 \leq j \leq n+2} f_j. \tag{3.5}$$

Proof. Let us consider the left-hand side inequality in (3.5). In case $p_i = \min(f_0, f_{n+2})$ the inequality holds immediately. Thus, let us assume that $p_i < \min(f_0, f_{n+2})$. Then by definitions (2.2), (2.3) and the property (2.4) we have

$$\begin{aligned} p_i &= c_{i-1} f_{i-1} + c_i f_i + c_{i+1} f_{i+1} + c_{i+2} f_{i+2} + c_i' d_i + c_{i+1}' d_{i+1} \\ &= f_{\min} + c_{i-1}(f_{i-1} - f_{\min}) + c_i(f_i - f_{\min}) + c_{i+1}(f_{i+1} - f_{\min}) \\ &\quad + c_{i+2}(f_{i+2} - f_{\min}) + c_i' d_i + c_{i+1}' d_{i+1}. \end{aligned} \tag{3.6}$$

Here and in the sequel we denote $f_{\min} = \min_{0 \leq j \leq n+2} f_j$ and $f_{\max} = \max_{0 \leq j \leq n+2} f_j$.

Let us assume that $d_i \neq 0$ or $d_{i+1} \neq 0$ (otherwise (3.5) follows directly from (3.6) and (3.1)). Then, the following cases are possible for $\varrho = \frac{8}{3}$:

1. If $d_i = 0$ and $d_{i+1} \neq 0$ then assuming $f_i = f_{\min}$, we have by (3.6), (2.6), and (3.2a)

$$\begin{aligned} p_i &\geq f_{\min} + c_{i+1}(f_{i+1} - f_{\min}) + c_{i+2}(f_{i+2} - f_{\min}) \\ &\quad + \varrho c_{i+1}' \min(|\Delta_i|, |\Delta_{i+1}|) \\ &\geq f_{\min} + (c_{i+1} + 2c_{i+2} + \varrho c_{i+1}') \min(|\Delta_i|, |\Delta_{i+1}|) \geq f_{\min}, \end{aligned} \tag{3.7}$$

since the data are increasing at x_{i+1} (note that the case f_i – local maximum is trivial, and $f_{i+1} = f_{\min}$ contradicts the condition $d_{i+1} \neq 0$).

2. If $d_i \neq 0$ and $d_{i+1} = 0$ then putting $f_{i+1} = f_{\min}$, we get by (3.6), (2.6), and (3.2b)

$$\begin{aligned} p_i &\geq f_{\min} + c_{i-1}(f_{i-1} - f_{\min}) + c_i(f_i - f_{\min}) \\ &\quad - \varrho c_i' \min(|\Delta_{i-1}|, |\Delta_i|) \\ &\geq f_{\min} + (2c_{i-1} + c_i - \varrho c_i') \min(|\Delta_{i-1}|, |\Delta_i|) \geq f_{\min}, \end{aligned} \tag{3.8}$$

since the data are decreasing at x_i.

3. If $d_i \neq 0$ and $c_{i+1} \neq 0$ (the data are strictly monotone) then by (3.1), (3.3), (3.6), and the same technique as that used in the previous estimates, we get

$$p_i \geq f_{\min} + [c_i + c_{i+1} - \varrho(c_i' - c_{i+1}')] \min(|\Delta_i|, |\Delta_{i+1}|) \geq f_{\min}.$$

This completes the proof of the left inequality in (3.5). The right-hand side inequality can be proved similarly. ∎

PROPOSITION 3.2. *Let the assumptions of* Proposition 3.1 hold. If $\varrho = 3.5$, *then the interpolant* (2.2) *is positive definite for strictly monotone data and admits limited under- or overshootings in the neighborhood of extremum points.*

Proof. Let us assume that the data are strictly monotone in $[x_i, x_{i+1}]$; that means $d_i \neq 0$ and $d_{i+1} \neq 0$ (as well as $f_i, f_{i+1} > f_{\min}$). Thus, by (3.3), the right-hand side of the inequality (3.6) can be estimated as

$$\begin{aligned} p_i &\geq f_{\min} + c_i(f_i - c_{\min}) + c_{i+1}(f_{i+1} - f_{\min}) \\ &\quad - \varrho c_i' \min(|\Delta_{i+1}|, |\Delta_i|) + \varrho c_{i+1}' \min(|\Delta_i|, |\Delta_{i+1}|) \\ &\geq f_{\min} + (c_i + c_{i+1} - \varrho c_i' + \varrho c_{i+1}') \min(|\Delta_i|, |\Delta_{i+1}|) \geq f_{\min}. \end{aligned}$$

This implies the left inequality of (3.5), and the right-hand side can be proved in the same way.

In the neighborhood of the minimum, the maximum principle holds in the case $f_i = f_{i+1} = f_{\min}$. Otherwise we have $(f_i = f_{\min}) \wedge (d_{i+1} \neq 0)$ or $(f_{i+1} = f_{\min}) \wedge (d_i \neq 0)$ and the arguments used in the proof of Proposition 3.1 can be applied. Utilizing estimates (3.7) and (3.8), as well as inequalities (3.4) in the respective cases, we get the left of the following inequalities (the right-hand side inequality can be obtained in a similar way):

$$f_{\min} - 0.0305 \max[\min(|\Delta_{i-1}|, |\Delta_i|), \min(|\Delta_i|, |\Delta_{i+1}|)] \le p_i \le f_{\max} + 0.0305 \max[\min(|\Delta_{i-1}|, |\Delta_i|), \min(|\Delta_i|, |\Delta_{i+1}|)].$$

This completes the proof. ∎

The formulated results state that the scheme is positive definite for $\varrho = \frac{8}{3}$, but it can also be useful for the limiter coefficient up to about $\varrho = 3.5$, especially in regular data and flat gradient cases. Note that the proofs remain valid for local extrema.

4. MONOTONICITY CONDITIONS

Before discussing the monotonicity of (2.2) let us recall the basic definitions [10, 17]. The data are *nondecreasing at* x_i if $f_{i-1} \le f_i \le f_{i+1}$ and they are *nondecreasing in* $[x_i, x_{i+1}]$ if they are nondecreasing at x_i and x_{i+1}. Analogous definitions hold for nonincreasing data. The data are *monotone at* x_i (or *in* $[x_i, x_{i+1}]$) if they are nondecreasing or nonincreasing at x_i (or *in* $[x_i, x_{i+1}]$). Consequently, the interpolant *pf* is *monotone in* $[x_i, x_{i+1}]$ if the values $(pf)(x)$ are monotone for all $x \in [x_i, x_{i+1}]$.

In general, the monotonicity of (2.2) can be characterized as the respective subset of R^4 (compare [4]) depending on four parameters $(d_i, d_{i+1}, f_{i-1}, f_{i+2})$. In the case of the quintic considered, there exists a relation between them due to the definition of the derivative estimates. To formulate monotonicity conditions we develop a technique applied in [10] for cubics and consider four auxiliary quintic polynomials $h_{(d_i,d_{i+1})}(\alpha; f_{i-1}, f_{i+2})$ that characterize the desired properties of (2.2).

Thus, assume that the data are nondecreasing in $[x_i, x_{i+1}]$, i.e., $f_{i-1} \le f_i \le f_{i+1} \le f_{i+2}$. In the case $f_i = f_{i+1}$, the monotonicity of *pf* follows directly from (2.2) and (2.6e). If $f_i \neq f_{i+1}$, without loss of generality we can put $f_i = 0$ and $f_{i+1} = 1$. As discussed in [10], it can be formally obtained by linear transformation of the coordinates in (2.2)–(2.3),

$$\tilde{y} = (y(\alpha) - f_i)/(f_{i+1} - f_i), \tag{4.1}$$

where (α, y) is the original coordinate system for $\alpha \in [0, 1]$.

Let the assumptions of Proposition 3.1 hold for the limiter constant $\rho = \frac{8}{3}$ in (2.6). Following the approach of Huynh [10], we shall consider four pairs of derivative estimates, $(d_i, d_{i+1}) = (0, 0), (\frac{8}{3}, 0), (0, \frac{8}{3}), (\frac{8}{3}, \frac{8}{3})$. Denoting, for simplicity, the respective polynomials by $h_{(0,0)} = h_{(0,0)}(\alpha; 0, 1)$, $h_{(3,0)} = h_{(3,0)}(\alpha; f_{i-1}, 1)$, $h_{(0,3)} = h_{(0,3)}(\alpha; 0, f_{i+2})$, and $h_{(3,3)} = h_{(3,3)}(\alpha; f_{i-1}, f_{i+2})$, we have by (2.2)

$$\begin{aligned}
h_{(0,0)} &= c_{i+1}(\alpha) + c_{i+2}(\alpha), \quad (f_{i-1}, f_{i+2}) \in \{0\} \times \{1\},\\
h_{(3,0)} &= c_{i-1}(\alpha) f_{i-1} + c_{i+1}(\alpha) + c_{i+2}(\alpha)\\
&\quad + \tfrac{8}{3} c'_i(\alpha), \quad (f_{i-1}, f_{i+2}) \in (-\infty, -1] \times \{1\},\\
h_{(0,3)} &= c_{i+1}(\alpha) + c_{i+2}(\alpha) f_{i+2}\\
&\quad + \tfrac{8}{3} c'_{i+1}(\alpha), \quad (f_{i-1}, f_{i+2}) \in \{0\} \times [2, \infty),\\
h_{(3,3)} &= c_{i-1}(\alpha) f_{i-1} + c_{i+1}(\alpha) + c_{i+2}(\alpha) f_{i+2}\\
&\quad + \tfrac{8}{3} [c'_i(\alpha) + c'_{i+1}(\alpha)], \quad (f_{i-1}, f_{i+2}) \in (-\infty, -1] \times [2, \infty),
\end{aligned} \tag{4.2}$$

where coefficients $c_i(\alpha)$, $c'_i(\alpha)$ are defined by (2.3) for $\alpha \in [0, 1]$. Observe that the domains of parameters (f_{i-1}, f_{i+2}) in the respective functions result from the monotonicity of the data in $[x_i, x_{i+1}]$ (and $f_i = 0$, $f_{i+1} = 1$), as well as from condition (2.6d).

If the polynomials (4.2) are increasing in $[0, 1]$ then any linear combination of them with positive coefficients is also increasing. Let (d_i, d_{i+1}) be an arbitrary pair of slopes that satisfy (2.6d) for $\rho = \frac{8}{3}$, with the respective grid values (f_{i-1}, f_{i+2}). Then, one can subsequently calculate (compare [10])

$$\begin{aligned}
h_{(d_i,0)} &= \tfrac{3}{8} d_i h_{(3,0)} + (1 - \tfrac{3}{8} d_i) h_{(0,0)},\\
h_{(d_i,3)} &= \tfrac{3}{8} d_i h_{(3,3)} + (1 - \tfrac{3}{8} d_i) h_{(0,3)},\\
h_{(d_i,d_{i+1})} &= \tfrac{3}{8} d_{i+1} h_{(d_i,3)} + (1 - \tfrac{3}{8} d_{i+1}) h_{(0,0)}.
\end{aligned}$$

It follows from (4.2) that the last polynomial has a form

$$\begin{aligned}
\tilde{h}(\alpha) = h_{(d_i,d_{i+1})} &= c_{i-1}(\alpha) \tilde{f}_{i-1} + c_{i+1}(\alpha)\\
&\quad + c_{i+2}(\alpha) \tilde{f}_{i+2} + c'_i(\alpha) d_i + c'_{i+1}(\alpha) d_{i+1},
\end{aligned}$$

satisfies conditions $\tilde{h}(0) = 0$, $\tilde{h}(1) = 1$, $\tilde{h}'(0) = d_i$, $\tilde{h}'(1) = d_{i+1}$, and moreover,

$$\tilde{f}_{i-1} = \tfrac{3}{8} d_i f_{i-1}; \quad \tilde{f}_{i+2} = 1 + \tfrac{3}{8} d_{i+1} (f_{i+2} - 1). \tag{4.3}$$

As a consequence, the set (4.2) maps the domain of parameters (f_{i-1}, f_{i+2}): $(-\infty, -1] \times [2, \infty)$ onto $(-\infty, 0] \times [1, \infty)$ for $(d_i, d_{i+1}) \in [0, \frac{8}{3}] \times [0, \frac{8}{3}]$. Specifically, it follows from (4.3) that any arbitrary pair of parameters $(\tilde{f}_{i-1}, \tilde{f}_{i+2}) \in (-1, 0] \times [1, 2)$ can be obtained as a convex combination of auxiliary polynomials for the slopes

$$\tilde{d}_i = \frac{8}{3} \frac{\tilde{f}_{i-1}}{f_{i-1}}, \quad \tilde{d}_{i+1} = \frac{8}{3} \frac{\tilde{f}_{i+2} - 1}{f_{i+2} - 1}. \tag{4.4}$$

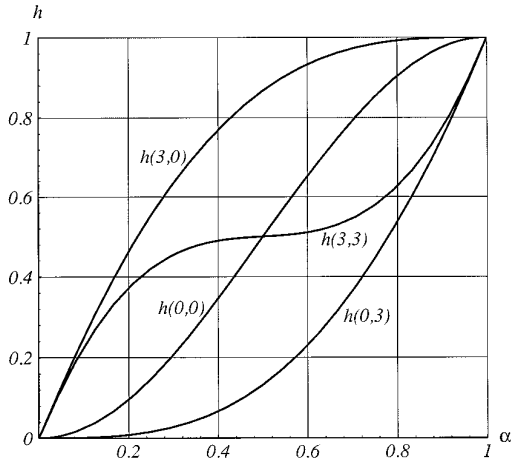

FIG. 1. Auxiliary polynomials for $f_{i-1} = 0$ and $f_{i+2} = 1$.

Thus, in the following the domain of polynomials (4.2) can be extended by continuity to $(-\infty, 0] \times [1, \infty)$. They will be utilized to characterize the monotonicity of (2.2); the respective conditions will be formulated in terms of the monotonicity region of parameters (f_{i-1}, f_{i+2}). In Fig. 1 plots of $h_{(0,0)}(\alpha)$, $h_{(3,0)}(\alpha)$, $h_{(0,3)}(\alpha)$, and $h_{(3,3)}(\alpha)$ are shown for $0 \le \alpha \le 1$ and the fixed values of parameters $(f_{i-1}, f_{i+2}) = \{0, 1\}$. It can be seen that the functions are (strictly) increasing in (0, 1) (the respective derivatives are positive). The first one is uniquely determined and the others are discussed below.

To determine the monotonicity regions for $h_{(3,0)}$ and $h_{(0,3)}$ the derivatives (with respect to α) can be considered. It follows from (4.2) and (2.3) that they have a form

$$\begin{aligned} h'_{(3,0)}(\alpha; f_{i-1}) &= \tfrac{1}{12}(1-\alpha)[32 - 2\alpha(1 - 2f_{i-1}) \\ &\quad - \alpha^2(62 + 11f_{i-1}) + 5\alpha^3(6 + f_{i-1})], \\ h'_{(0,3)}(\alpha; f_{i+2}) &= \tfrac{1}{12}\alpha(-4 + 2f_{i+2} + 3\alpha(13 - f_{i+2}) \\ &\quad + 4\alpha^2(8 - f_{i+2}) - 5\alpha^3(7 - f_{i+2})]. \end{aligned} \tag{4.5}$$

The 3D plots of the above surfaces are shown in Fig. 2.

It can be seen that the minimum value

$$h_{\min}(f_{i-1}) = \min_{0 \le \alpha \le 1} h'_{(3,0)}(\alpha, f_{i-1})$$

is decreasing for $f_{i-1} \to -\infty$ and the lower bound of the monotonicity of $h_{(3,0)}$ can be found as

$$f^*_{i-1} = \arg\min_{h_{\min} \ge 0} h_{\min}(f_{i-1}).$$

This point was numerically evaluated as the solution of the set

$$[h'_{(3,0)}(\alpha; f_{i-1}) = 0] \wedge [h''_{(3,0)}(\alpha; f_{i-1}) = 0]$$

and the obtained lower bound coordinates are $\alpha^*_1 = 0.236695$ and $f^*_{i-1} = -71.69877931$ (accuracy $\varepsilon = 2.3\text{E} - 10$). In a similar way, the upper limit point of the monotonicity interval for $h_{(0,3)}$ was determined as the solution of

$$[h'_{(0,3)}(\alpha; f_{i+2}) = 0] \wedge [h''_{(0,3)}(\alpha; f_{i+2}) = 0].$$

It is $\alpha^*_2 = 0.7633043$, $f^*_{i+2} = 72.6983793$ for the same accuracy as above. The resulting plots of $h_{(3,0)}(\alpha; f^*_{i-1})$, $h'_{(3,0)}(\alpha; f^*_{i-1})$, $h_{(0,3)}(\alpha; f^*_{i+2})$, and $h'_{(0,3)}(\alpha; f^*_{i+2})$ are presented in Fig. 3.

By definition (4.2), the derivative of $h_{(3,3)}$ depends on two parameters and has the form

$$\begin{aligned} h'_{(3,3)}(\alpha; f_{i-1}, f_{1+2}) &= \tfrac{1}{12}[32 + 2\alpha(-50 + 2f_{i-1} + f_{i+2}) \\ &\quad - 3\alpha^2(3 + 5f_{i-1} + f_{i+2}) \\ &\quad + 4\alpha^3(56 + 4f_{i-1} - f_{i+2}) \\ &\quad - 5\alpha^4(23 + f_{i-1} - f_{i+2})]. \end{aligned} \tag{4.6}$$

We use this function to characterize the monotonicity of $h_{(3,3)}$ in a domain of parameters (f_{i-1}, f_{i+2}). Observe first that the symmetry property follows from (4.6):

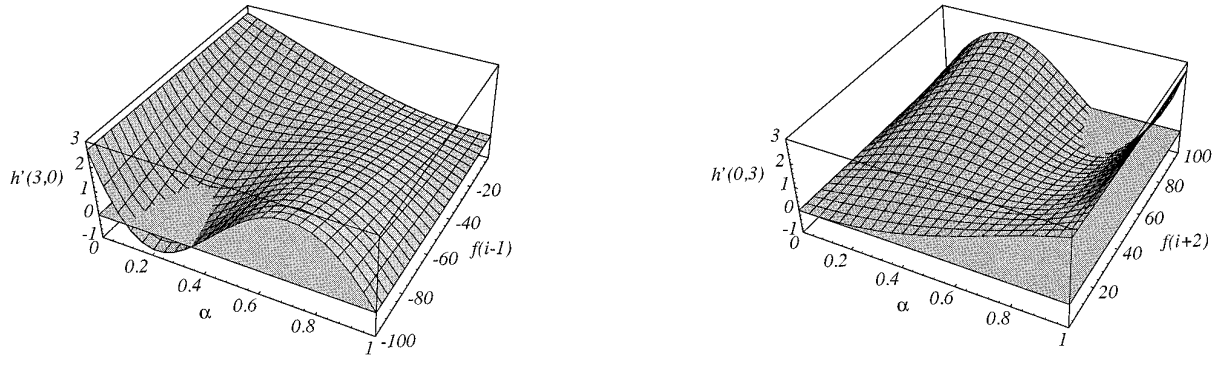

FIG. 2. Surfaces $h'_{(3,0)}(\alpha; f_{i-1})$ (left) and $h'_{(0,3)}(\alpha; f_{i+2})$ (right).

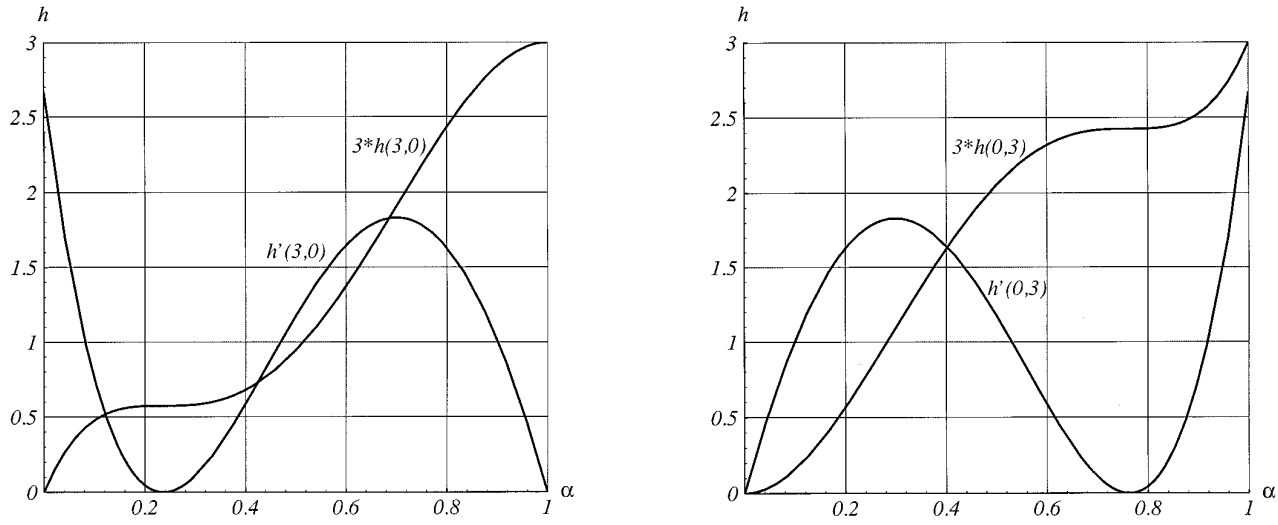

FIG. 3. Functions $h_{(3,0)}(\alpha; f^*_{i-1})$, $h'_{(3,0)}(\alpha; f^*_{i-1})$(left) and $h_{(0,3)}(\alpha; f^*_{i+2})$, $h'_{(0,3)}(\alpha; f^*_{i+2})$ (right) for monotonicity limit values of parameters.

$$h'_{(3,3)}(\alpha; f_{i-1}, f_{i+2}) = h'_{(3,3)}(1-\alpha; 1-f_{i+2}, 1-f_{i-1}). \quad (4.7)$$

Thus, the analysis can be limited to a subdomain bounded by the straight lines:

$$f_{i+2} = 1, \quad f_{i-1} + f_{i+2} = 1.$$

It follows from (4.6) that the derivative $h'_{3,3}$ has in those cases the form

$$\begin{aligned} h'_{(3,3)}(\alpha; f_{i-1}, 1) = \tfrac{1}{12}\,[&32 - 2\alpha(49 - 2f_{i-1}) \\ &- 3\alpha^2(4 - 3f_{i-1}) + 4\alpha^3(55 + 4f_{i-1}) \\ &- 5\alpha^4(22 + f_{i-1})], \end{aligned} \quad (4.8)$$

$$\begin{aligned} h'_{(3,3)}(\alpha; f_{i-1}, 1 - f_{i-1}) = \tfrac{1}{6}\,[&16 - \alpha(49 - f_{i-1}) - 6\alpha^2(1 + f_{i-1}) \\ &+ 10\alpha^3(11 + f_{i-1}) - 5\alpha^4(11 + f_{i-1})]. \end{aligned}$$

The respective surfaces, presented in Fig. 4, show the regions of derivative nonnegativity in both cases. The exact coordinates of the characteristic points that indicate regions of derivative nonnegativity were calculated in the same way as those of (4.5). They are

P_1. $(f_{i-1}, f_{i+2}) = (-21.94, 1)$ for the straight line $f_{i+2} = 1$ and

P_2. $(f_{i-1}, f_{i+2}) = (-191, 192)$ for the straight line $f_{i-1} + f_{i+2} = 1$.

The respective branch of the monotonicity region for $h_{(3,3)}$, connecting the above points, was numerically found by the bisection method. Relation (4.7) was used to find a symmetric branch connecting P_2 with

P_3. $(f_{i-1}, f_{i+2}) = (0, 22.94)$ for the straight line $f_{i-1} = 0$.

The monotonicity limits for the auxiliary polynomials (4.2) and the resulting monotonicity region for (2.2) are presented in Fig. 5.

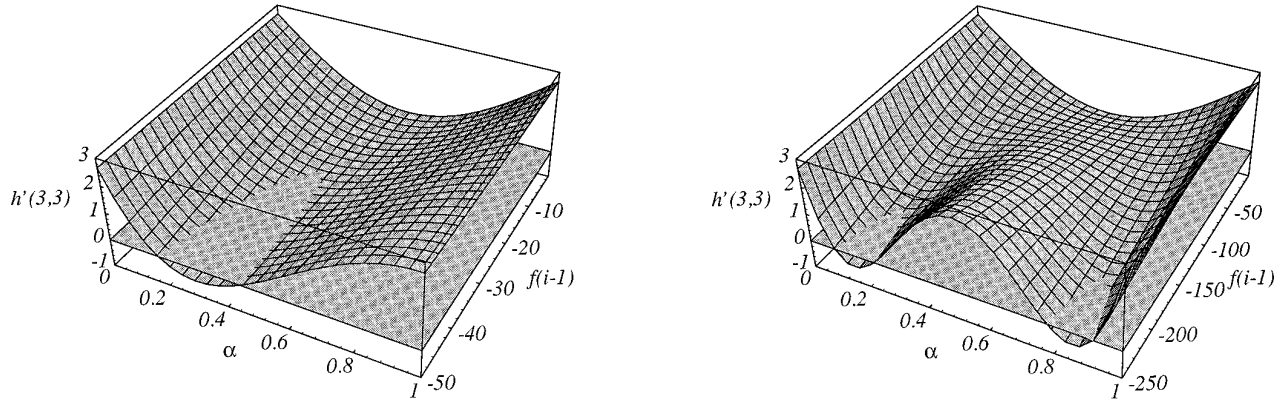

FIG. 4. Surfaces $h'_{(3,3)}(\alpha; f_{i-1}, 1)$ (left) and $h'_{(3,3)}(\alpha; f_{i-1}, 1 - f_{i-1})$ (right).

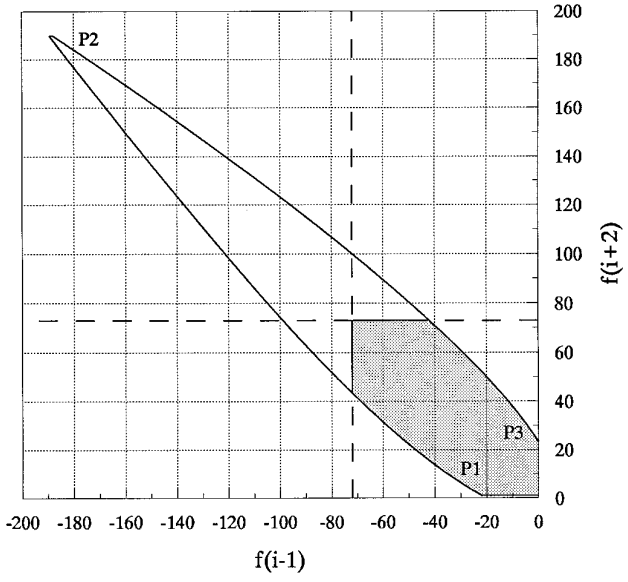

FIG. 5. Monotonicity region for interpolant $p(x)$.

Results of this section can be summarized as the following.

PROPOSITION 4.1. *The interpolant* (2.2) *with the coefficients defined by* (2.3) *and the limiter constant* $\varrho = \frac{8}{3}$ *in* (2.6d) *is monotone in* $[x_i, x_{i+1}]$, *provided that the grid values* (f_{i-1}, f_{i+2}) *are in the domain shown in Fig.* 5.

5. IMPLEMENTATION AND LIMITER FUNCTIONS

The interpolation method discussed was implemented for several algorithms of derivative estimates, known from the literature. Results of the numerical tests presented in the next section refer to Fritsch and Butland (FB), Akima (AK), and "Superbee" (SB) methods [6, 10, 17], which are defined as follows:

$$\text{FB.}\quad d_i = \begin{cases} \dfrac{3\Delta_{i-1}\Delta_i}{2|\Delta_{i-1}| + |\Delta_i|}, & (\Delta_{i-1}\Delta_i > 0) \wedge (|\Delta_{i-1}| \le |\Delta_i|), \\ \dfrac{3\Delta_{i-1}\Delta_i}{|\Delta_{i-1}| + |2\Delta_i|}, & (\Delta_{i-1}\Delta_i > 0) \wedge (|\Delta_{i-1}| > |\Delta_i|), \\ 0, & \Delta_{i-1}\Delta_i \le 0, \end{cases}$$

$$\text{AK.}\quad d_i = \begin{cases} \dfrac{\alpha\Delta_{i-1} + \beta\Delta_i}{\alpha + \beta}, & \alpha + \beta \ne 0, \\ \dfrac{\Delta_{i-1} + \Delta_i}{2}, & \alpha + \beta = 0, \end{cases}$$

$$\text{SB.}\quad d_i = \gamma \min[\max(|\Delta_{i-1}|, |\Delta_i|), 3\min(|\Delta_{i-1}|, |\Delta_i|)],$$

where the discrete slope is $\Delta_i = (f_{i+1} - f_i)/h$ and the coefficients in the last two formulas are $\alpha = |\Delta_{i+1} + \Delta_i|$, $\beta = |\Delta_{i-1} + \Delta_{i-2}|$, and $\gamma = 0.5 \cdot [\operatorname{sgn}(\Delta_{i-1}) + \operatorname{sgn}(\Delta_i)]$, respectively.

It is well known that the monotonicity constraints of a general form (2.6) cause loss of accuracy, mainly by generating "too flat" solutions near strict local extrema. This effect follows from the property that the interpolant is still monotone in the neighborhood of the extremum, even though the data are not.

One of the methods of overcoming this drawback and increasing the overall accuracy is to relax the monotonicity constraints in the vicinity of the local extremum and replace them by higher order approximation. We consider here the parabolic interpolation scheme discussed in [10]. This is a rather natural approach in the case of a four-point interpolation scheme (2.2), since the points f_{i-1}, f_i, f_{i+1} can be utilized to approximate d_i and f_i, f_{i+1}, f_{i+2}, to approximate d_{i+1}, respectively.

The approximation method proposed in [10] utilizes a parabola and its derivative,

$$\begin{aligned} s_{i+1/2}(x) &= f_i + \Delta_i(x - x_i) + \Delta^2_{i+1/2}(x_i)(x - x_i)(x - x_{i+1}), \\ s'_{i+1/2}(x) &= \Delta_i + \Delta^2_{i+1/2}(2x - x_i - x_{i+1}), \end{aligned} \tag{5.1}$$

where $\Delta^2_i = (\Delta_{i+1} - \Delta_i)/(2h)$ and $\Delta^2_{i+1/2} = \operatorname{minmod}(\Delta^2_i, \Delta^2_{i+1})$. It is shown in [10] that (5.1) preserves the monotonicity of the data, and the respective accuracies are

$$s_{i+1/2}(x) = f(x) + O(h^3), \quad s'_{i+1/2}(x) = f'(x) + O(h^2).$$

The resulting algorithm of the parabolic approximation to d_i consists of the computational steps

$$s'_{i-1/2} = \Delta_{i-1} + \Delta^2_{i-1/2}(x_i)(x_i - x_{i-1}), \tag{5.2a}$$

$$s'_{i+1/2} = \Delta_i + \Delta^2_{i+1/2}(x_i)(x_i - x_{i+1}), \tag{5.2b}$$

$$t_i = \operatorname{minmod}(s'_{i-1/2}, s'_{i+1/2}), \tag{5.2c}$$

$$t_{\max} = \operatorname{sgn}(t_i)\max[3|\operatorname{minmod}(\Delta_{i-1}, \Delta_i)|, \tfrac{3}{2}|t_i|], \tag{5.2d}$$

$$d_i = \operatorname{minmod}(d_i^0, t_{\max}), \tag{5.2e}$$

where d_i^0 is the original derivative estimate obtained by any standard, lower order method. Approximation of d^0_{i+1} is calculated in the same way.

However, replacing the monotonicity constraints by (5.2) in the vicinity of local extrema may cause scheme (2.2) to no longer be positive definite, which is an essential property in most applications. To avoid such cases, an additional computational step is performed near the extremum points. It is based upon verification of the discrete maximum principle conditions and the respective reduction of the coefficient $\frac{3}{2}$ in formula (5.2d), if the scheme is not positive definite. To this end, if $f_i = f_{\min}$ (where $f_{\min}$ is a local minimum) the following condition is verified (compare the proof of Proposition 3.1):

$$\begin{aligned} r_i = c_{i-1}(f_{i-1} - f_{\min}) + c_{i+1}(f_{i+1} - f_{\min}) \\ + c_{i+2}(f_{i+2} - f_{\min}) \ge -c'_{i+1}t_{i+1}. \end{aligned}$$

If the inequality does not hold, the coefficient $\frac{3}{2}$ in (5.2d) is multiplied by the factor

$$\rho_i = r_i/(c'_{i+1}t_{i+1}), \quad 0 \le \rho_i \le 1. \tag{5.3}$$

In the case $f_{i+1} = f_{\min}$ the respective inequality is

$$r_{i+1} = c_{i-1}(f_{i-1} - f_{\min}) + c_i(f_i - f_{\min}) + c_{i+2}(f_{i+2} - f_{\min}) \ge -c'_i t_i,$$

and the correction factor has the form

$$\rho_{i+1} = r_{i+1}/(c'_i t_i), \quad 0 \le \rho_{i+1} \le 1. \tag{5.4}$$

Analogous correction steps are performed in the neighborhood of the maximum.

The derivative estimate functions defined at the beginning of this section, combined with the parabolic interpolation method, will be denoted FB2, AK2, and SB2, respectively. In those implementations, the original method is applied for calculation of the initial approximation, d_i^0, which is next utilized in the parabolic interpolation algorithm (5.2). Numerical tests performed show that the correction steps (5.3), (5.4) are active near the strict local extrema or the input data discontinuities.

The interpolation algorithm discussed in the paper applies directly to the interior points. To obtain consistency with the boundary conditions, the high-order constraints should be replaced by appropriate lower-order ones near the boundaries. Due to the symmetry of the interpolation scheme, only one type of boundary conditions (left) is considered in the sequel.

Specific implementation depends on the boundary conditions imposed. If f_0 is the boundary value at x_0, then f_{-1} can be estimated by the second-order extrapolation.

$$f_{-1} = \max(0, 3f_0 - 3f_1 + f_2). \tag{5.5}$$

Then, to calculate the derivative estimate d_0, any 3-point limiter function (e.g., Fritsch-Butland or "Superbee") may be used. Another possibility is to apply a one-sided parabolic approximation [10] of the form

$$\dot{f}_0 = \Delta_0 + \Delta_1^2(x_0 - x_1). \tag{5.6}$$

In this case, the necessary condition of monotonicity can be imposed as follows:

$$d_0 = \operatorname{minmod}(\dot{f}_0, 3\Delta_0). \tag{5.7}$$

The last constraint may clip the local extremum if it appears at the grid point next to the boundary.

Also cubic formulas [10] based on f_0, f_1, estimate (5.6), and (5.7) can be applied for the interpolation in $[x_0, x_1]$. Both approaches can also be adapted to the case where the derivative $\dot{f}_0$ is given as the boundary condition.

In the next section the results of several computational tests performed by the method discussed are presented. They refer to interpolation of the exponential bell profile, as well as to 1D and 2D advection problems.

6. NUMERICAL RESULTS

6.1. *Interpolation of a Regular Function*

In this section selected numerical results of the computational tests performed by the method discussed are presented. The first experiment deals with interpolation of the function $f(x) = e^{-x^2}$ on a closed interval, discretized with a uniform grid (compare [10]).

Figure 6 presents the results for the domain $[-2.8, 3.6]$ with resolution $n = 8$ and the data points location symmetric with respect to the maximum. The FB limiter represents here the first-order methods with monotonicity-preserving constraints of type (2.6) that clip the extremum. The higher order methods generate "visually pleasing" solutions that are positive and without spurious oscillations. The three methods produce similar solutions in the vicinity of the maximum, where the values are determined by a parabolic approximation algorithm (maximum 0.973). Near the base of the profile the individual influence of the derivative estimates can be observed. The FB2 method produces the most accurate and regular solution in this area.

In Fig. 7 similar results are shown for the interval $[-2.9, 3.5]$ and the nonsymmetric distribution of the data with respect to the maximum position. This case confirms the good properties of FB2 and AK2 methods, while the SB2 limiter produces more significant error near the base of the profile.

In Table I the values of the root mean square error on the interval $[-1.7, 1.9]$ of the form in [10],

$$E_{\mathrm{RMS}} = \left[\frac{1}{3.6}\int_{-1.7}^{1.9}((pf)(x) - e^{-x^2})^2\,dx\right]^{1/2},$$

are presented for the resolutions $n = 8, 16, 32, 64$. The results confirm that the FB2 implementation gives the most accurate solution, while the tendency to overshoot the maximum in the SB2 scheme degrades the overall accuracy.

6.2. *The Application to Advection Problems*

Interpolation scheme (2.2) has been applied for solving the advection equation by the method of characteristics,

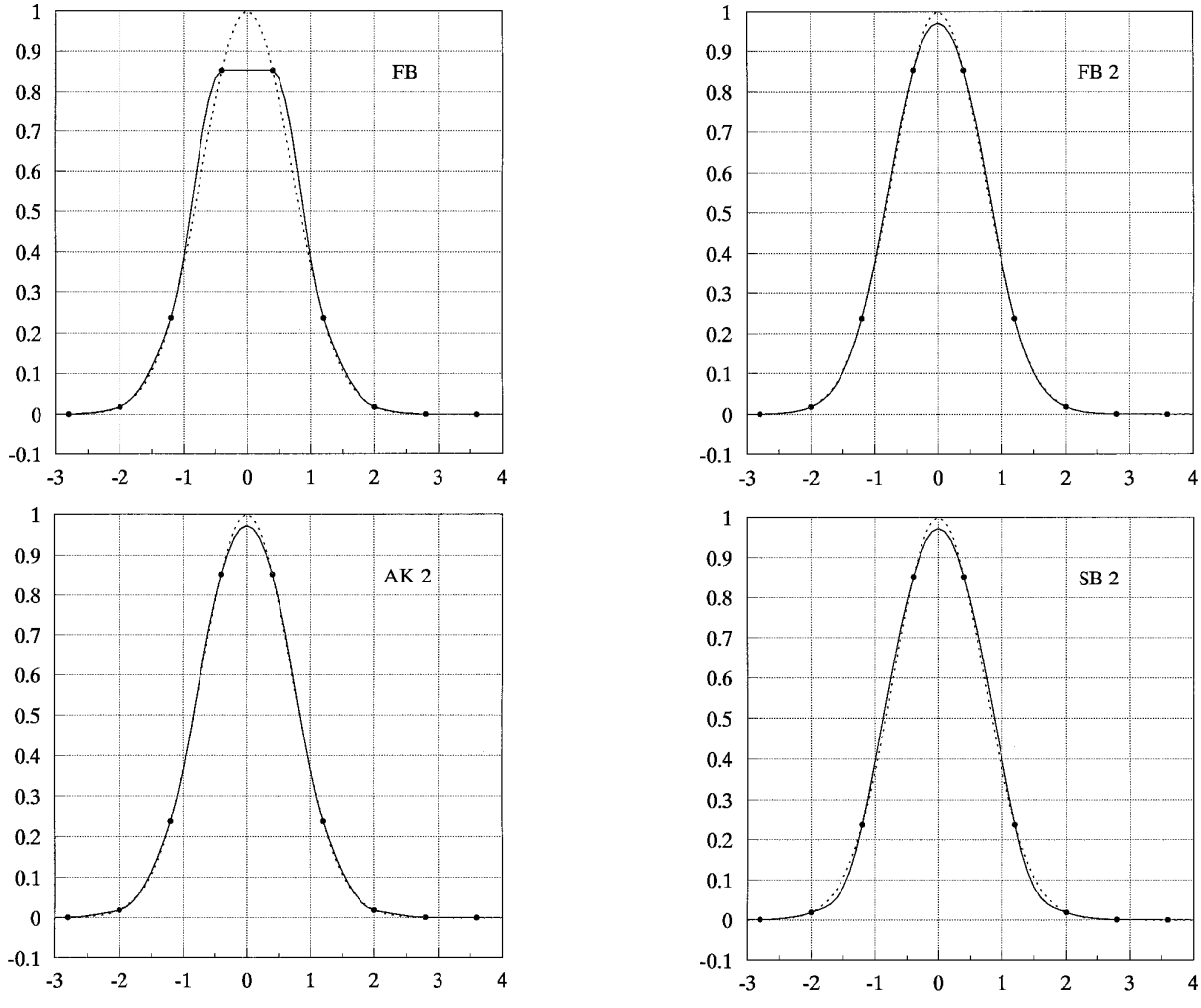

FIG. 6. Interpolation of $f(x) = \exp(-x^2)$ on the domain $[-2.8, 3.6]$.

combined with a uniform-grid spatial approximation (semi-Langrangian method). In the one-dimensional case a linear advection equation is considered,

$$\frac{\partial f}{\partial t} + u\,\frac{\partial f}{\partial x} = 0, \tag{6.1}$$

where $f(x, t)$ is a transported scalar quantity and $u(x, t)$ denotes the x-component of the wind vector. Let τ denote the time resolution step and h, the grid spacing. The method is based on integrating over the wind trajectory the profile that arrives at a grid point P at time $(n + 1)\tau$

$$f_P^{n+1} = f_*^n,$$

where f_*^n is the value of the factor f at the departure point x_* at time $n\tau$ (see [8] for details of the numerical scheme construction).

Estimation of the departure profile f_*^n is an essential step of this approach. It can be obtained by polynomial interpolation, utilizing the known values at the grid points. In this case, the interpolation parameter in (2.2) is determined as

$$\alpha = C - p \quad (0 \le \alpha \le 1),$$

where $C = u\tau/h$ is the Courant number and p is a parameter (integer number) that indicates how many grid steps upstream from the arrival point the interpolation interval lies [1, 8].

Shape-preserving properties of the interpolation method can be verified by the advection experiment of standard test functions. In Fig. 8 the resulting profiles for rectangle and triangle initial shapes of the base length $\lambda = 12h$ are presented. Both are obtained after 200 time steps, by FB, FB2, AK2, and SB2 interpolation algorithms, combined

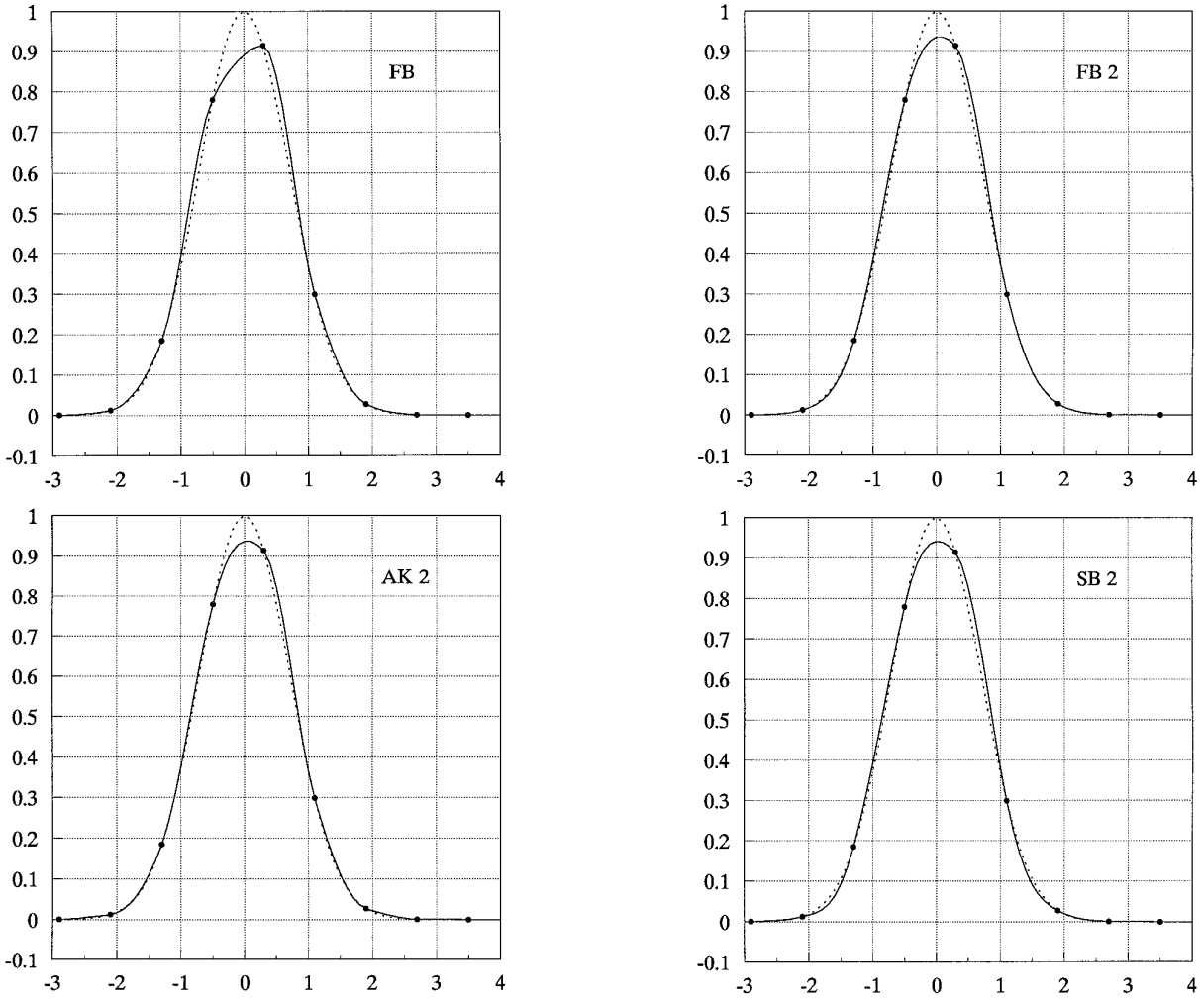

FIG. 7. Interpolation of $f(x) = \exp(-x^2)$ on the domain $[-2.9, 3.5]$.

with the method of characteristics defined above (Courant number $C = 3.2$). The results confirm good accuracy of FB2 algorithm. The SB2 method reproduces well rectangular profiles but it shows some overshoots of the maximum in the case of triangular functions.

The semi-Lagrangian advection method can be extended easily to the two-dimensional case by use of the directional split or tensor product [17]. We consider here two examples of rotating profiles that are commonly used in the literature [2, 3, 8, 9, 11–15]. The first test function represents a unit amplitude cone rotating in an advection field of constant angular velocity. It is considered in the square domain $[0, 1] \times [0, 1]$ discretized with step $h = 0.01$. The initial profile of radius $r_0 = 15h$, centered at (0.25, 0.5) is placed on a constant background equal to 25. One rotation of the cone is completed after 60 time steps.

TABLE I

Root Mean Square Errors for $f(x) = \exp(-x^2)$

Method	n = 8	n = 16	n = 32	n = 64
FB	2.8E-2	9.4E-4	1.1E-4	1.7E-5
FB2	5.7E-3	8.5E-4	7.5E-5	7.3E-6
AK2	5.0E-3	1.6E-3	9.5E-5	1.0E-5
SB2	9.5E-3	1.8E-3	1.3E-4	1.2E-5

Figure 9 shows the results of a simulation obtained after six revolutions by the AK2 and FB2 methods. The profile in both cases is accurately placed, with good shape preserving and very low clipping effect (the maximum values are 0.98 and 0.97, respectively). Regularity of the solution is remarkably good in the case of the FB2 method.

Quantitative evaluation of the accuracy in the case considered can be obtained by standard error measures [2, 11, 16]. Given a function f and its approximate solution F,

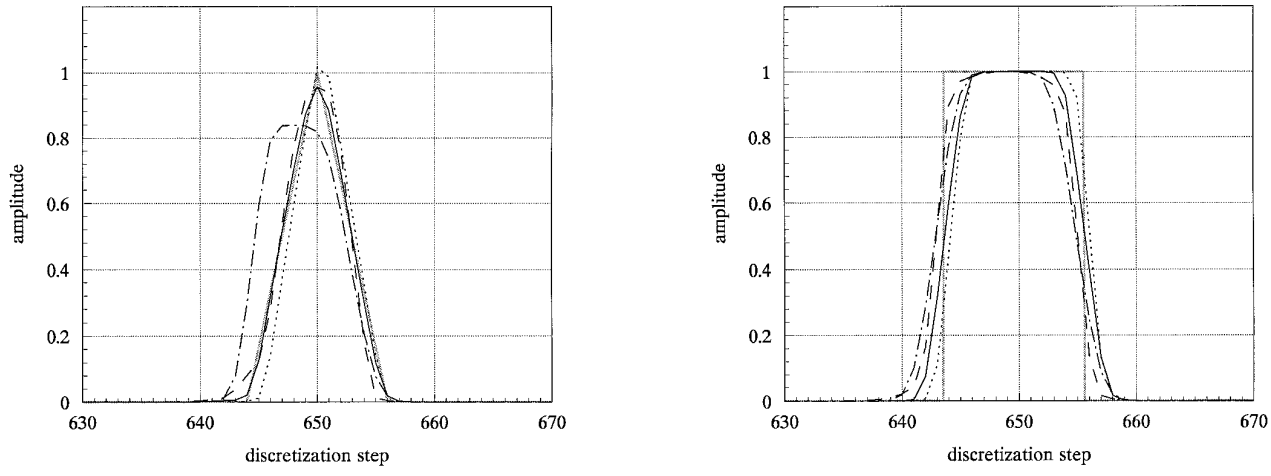

FIG. 8. Advection of a triangle (left) and a rectangle (right) after 200 time steps (–·–·, FB; – – –, AK2; ———, FB2; ···, SB2).

calculated on the set of K grid points, the mean-square error is defined as

$$\|f - F\|_h^2 = \frac{1}{K} \sum_k (f_k^n - F_k^n)^2,$$

for the nth time step. It can be shown [16] that the error is a sum of the dissipation error and the dispersion error,

$$\|f - F\|_h^2 = E_{\mathrm{DISS}} + E_{\mathrm{DISP}},$$

where

$$E_{\mathrm{DISS}} = [\sigma(f) - \sigma(F)]^2 + (\overline{f} - \overline{F})^2,$$
$$E_{\mathrm{DISP}} = 2(1 - \rho)\sigma(f)\sigma(F).$$

Here $\overline{f}$ and $\sigma(f)$ denote the mean and the variance, respectively. The correlation coefficient between functions f and F on the set of grid points is denoted by ρ.

Error estimates for two cases of the rotating cone experiment are presented in Table II and Table III. They can be compared with similar tests considered, for example, in [3] for flux-corrected transport, in [9] for the high order finite difference approximation, or in [2, 8, 11, 15] for semi-Langrangian advection. Generally, the obtained accuracy

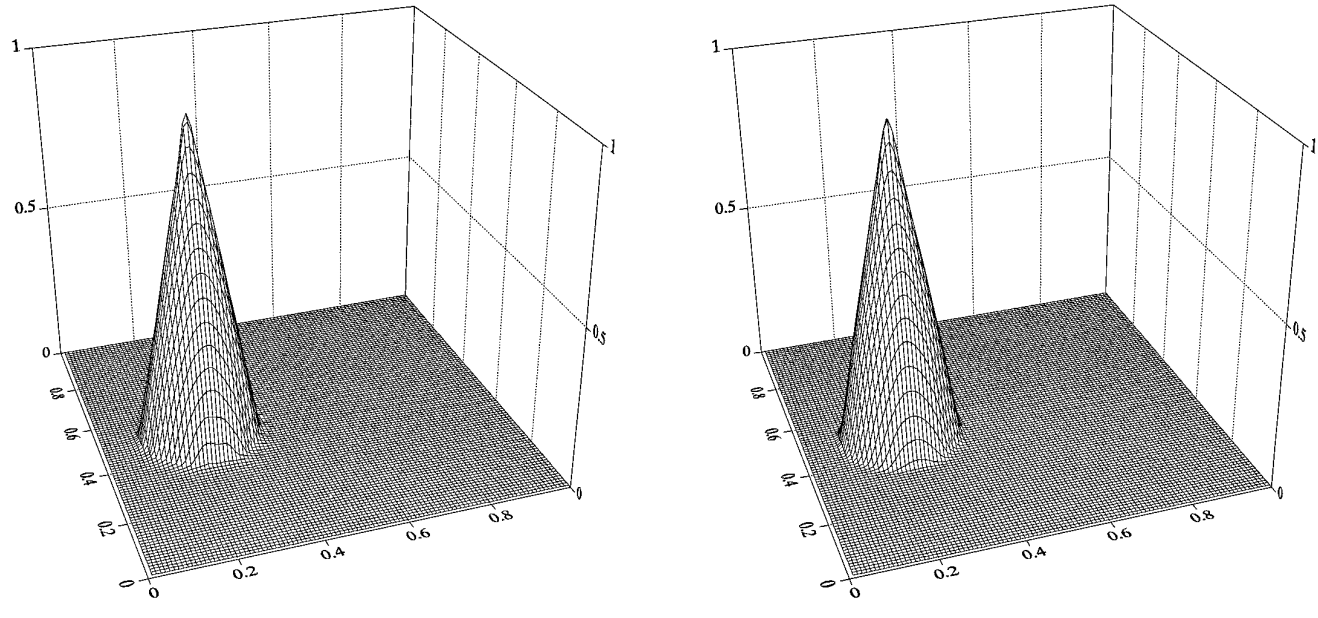

FIG. 9. Rotating cone after six revolutions by AK2 (left) and FB2 (right) methods.

TABLE II

Errors for the Rotating Cone Experiment by the AK2 Method

Time steps	$\int F / \int f_o$	$\int F^2 / \int f_o^2$	max(F)	min(F)	E_{DISS}	E_{DISP}
60	1.0001	1.0001	0.9662	0.0	0.6206E-06	0.6765E-05
120	1.0002	1.0007	0.9675	0.0	0.6312E-06	0.9192E-05
180	1.0002	1.0013	0.9695	0.0	0.6317E-06	0.1302E-04
240	1.0006	1.0018	0.9723	0.0	0.6638E-06	0.1781E-04
300	1.0010	1.0025	0.9753	0.0	0.7018E-06	0.2318E-04
360	1.0015	1.0031	0.9783	0.0	0.7372E-06	0.2925E-04

seems to be satisfactory, and the main relevance of the approach discussed is related to good shape preserving, with minor diffusion and very low clipping of the cone maximum.

Another two-dimensional computational example concerns the rotation of a slotted cylinder (compare [2, 8, 11, 14]). The initial profile forms a cylinder with height equal to 4, radius $r_0 = 15h$, and a center at (0.25, 0.5). The slot has the width 6h and the length $22h$. The resulting profile and its cross section at $y = 0.5$, obtained after six revolutions by the FB2 method are presented in Fig. 10.

The computed solution is positive, with no substantial diffusion and without overshoots. The slot and the top of the profile are reproduced very well, in comparison with other methods. The error measures presented in Table IV and Table V are comparable to, or better than, similar results in the refernces quoted. It can also be seen that the method has quite satisfactory conservation properties.

7. SUMMARY

The paper contributes to the state-of-the-art in higher order interpolation methods, with the emphasis on shape-preserving properties [4, 8–10]. In this context, as extended, high-accuracy version of the quintic interpolant defined in [8] is considered, including nonnegativity and monotonicity analysis, as well as new numerical tests. The results formulated provide an insight into the intrinsic limitations of the algorithm and give more confidence in its use.

Nonnegativity conditions of two types are formulated in Proposition 3.1 and Proposition 3.2. They state that the scheme discussed is positive definite if the limiter constant in the derivative estimate function is $\varrho \leq \frac{8}{3}$. However, for $\varrho \leq 3.5$ the scheme is also positive definite for strictly monotonic data, and it admits very limited under- and overshoots of local extrema. Thus, it can be successfully applied for that value of ϱ, especially for smooth profiles and in flat gradient areas. This property has been confirmed by the numerical results presented.

In monotonicity analysis the approach applied by Huynh [10] for Hermite cubics is followed. Since the monotonicity region for quintics is, in general, a compact convex set in a four-dimensional hyperplane [4], it is very difficult to find its analytical form. However, the numerical approach applied in Section 4 allows us to characterize this region (Proposition 4.1) and it can be easily implemented as a computational algorithm.

Numerical tests performed for three implementations of the derivative estimates confirm good accuracy of the interpolant and very good shape-preserving properties in the simulation of the advection process. An essential gain of the overall accuracy is due to relaxing the standard, first-order monotonicity constraints in the vicinity of local extrema and replacing them by a parabolic approximation [10]. This can be seen by comparing the results presented in Section 6 with those of [8] or by comparing accuracy of the FB and FB2 algorithms.

There are essential differences in the accuracy and pre-

TABLE III

Errors for the Rotating Cone Experiment by the FB2 Method

Time steps	$\int F / \int f_o$	$\int F^2 / \int f_o^2$	max(F)	min(F)	E_{DISS}	E_{DISP}
60	1.0000	1.0002	0.9704	0.0	0.5853E-06	0.7175E-05
120	1.0000	1.0010	0.9720	0.0	0.5802E-06	0.9335E-05
180	1.0000	1.0017	0.9741	0.0	0.5950E-06	0.1281E-04
240	0.9999	1.0021	0.9734	0.0	0.6039E-06	0.1754E-04
300	0.9997	1.0024	0.9702	0.0	0.6049E-06	0.2352E-04
360	0.9995	1.0025	0.9689	0.0	0.6046E-06	0.3064E-04

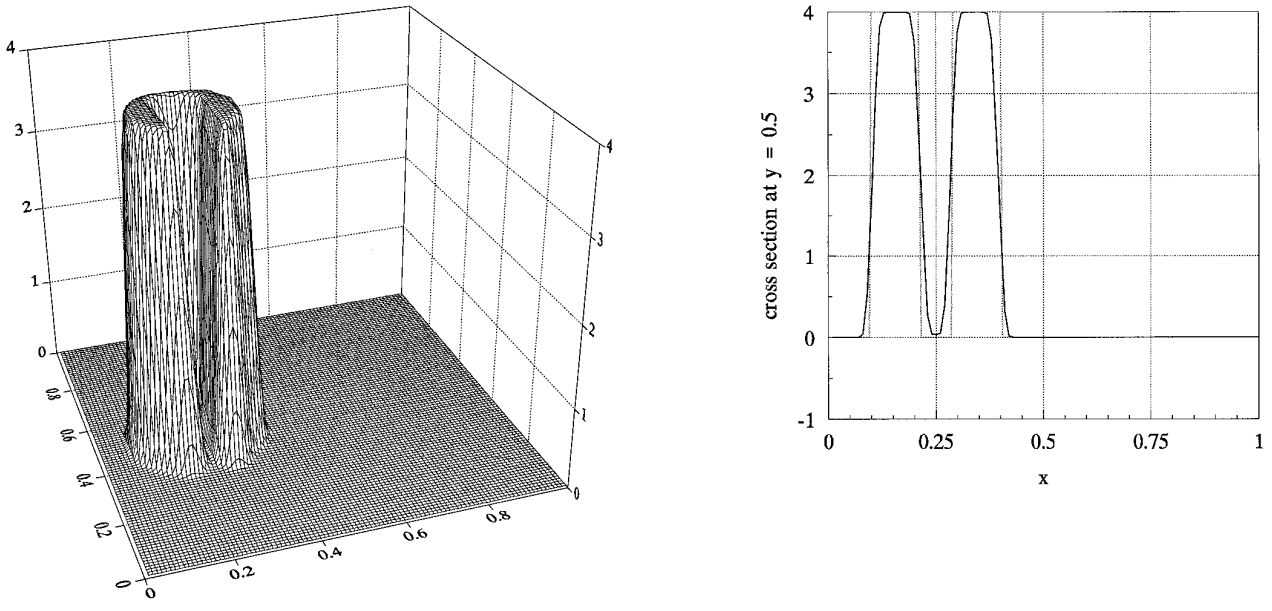

FIG. 10. Slotted cylinder after six revolutions by FB2 method and a cross section at $y = 0.5$.

serving the shape of the profile between the specific implementations of the derivative limiters. In the one-dimensional interpolation of an exponential function, the higher order versions generate the same solution near the maximum (due to the parabolic approximation routine) and they show the individual differences near the base of the profile. These differences are also reflected in the overall accuracy presented in Table I. The individual differences between the particular implementations are more evident in the approximation of the advection equation. The SB2 limiter represents well the rectangular profiles, but it shows overshoots for the triangle, which are significant in 2D cases. Implementations AK2, and SB2 in particular, well approximate the test function in both cases.

Results of the 2D advection tests can be compared with several other papers, where similar functions were considered [2, 3, 11–15]. In the rotating cone example, both the AK2 and SB2 methods show very good shape-preserving properties, low diffusivity, and minor maximum clipping effect. In this test case, the nonnegativity correction algorithm (5.3), (5.4) was active near the maximum of the cone, when using the AK2 method (the limiter constant $\varrho = 3$ was applied). The best regularity of the solution is obtained by the FB2 method, but in both implementations it is much better than that obtained in [8] for the standard Akima derivative estimate. The above facts are also seen in error measures presented in Table II and Table III.

Generally, the best results are obtained by combining interpolant (2.2) with the Fritsch–Butland limiter and parabolic approximation near the extremum FB2. Remarkably good shape-preserving properties of this implementation are seen clearly in the slotted cylinder experiment. The profile obtained after six revolutions is well centered, with low diffusion, and both the width of the upper face of the lobes and the depth of the slot are very well represented (see Fig. 10). In this case, due to the complicated shape of the profile the positivity correction step was performed near the slot of the cylinder.

TABLE IV

Errors for the Slotted Cylinder Experiment by the AK2 Method

Time steps	$\int F / \int f_o$	$\int F^2 / \int f_o^2$	max(F)	min(F)	E_{DISS}	E_{DISP}
60	0.9995	0.8797	3.9999	0.0	3.632E-03	3.961E-02
120	0.9997	0.8686	3.9991	0.0	4.364E-03	4.389E-02
180	1.0003	0.8610	3.9976	0.0	4.913E-03	4.700E-02
240	1.0012	0.8550	3.9956	0.0	5.354E-03	5.025E-02
300	1.0021	0.8498	3.9932	0.0	5.777E-03	5.311E-02
360	1.0023	0.8453	3.9905	0.0	6.157E-03	5.560E-02

TABLE V

Errors for the Slotted Cylinder Experiment by the FB2 Method

Time steps	$\int F / \int f_o$	$\int F^2 / \int f_o^2$	max(F)	min(F)	E_{DISS}	E_{DISP}
60	0.9996	0.8817	4.0000	0.0	3.511E-03	4.120E-02
120	0.9990	0.8683	4.0000	0.0	4.377E-03	4.768E-02
180	0.9986	0.8601	4.0000	0.0	4.955E-03	5.182E-02
240	0.9985	0.8544	4.0000	0.0	5.382E-03	5.499E-02
300	0.9984	0.8500	4.0000	0.0	5.726E-03	5.774E-02
360	0.9983	0.8464	4.0000	0.0	6.017E-03	6.026E-02

The numerical results also show that the method discussed has good shock-capturing properties that can make it useful in some specific application areas, despite relatively higher computational cost.

ACKNOWLEDGMENTS

The research was supported by the Japan Society for the Promotion of Science, Grant JSPS/SP2/94145, and performed at the Faculty of Engineering, Osaka University, during the author's stay as a visiting scientist. The hospitality of Professor Yutaka Suzuki, his interest in this work, and his encouragement are especially acknowledged. The author is also indebted to the anonymous referees for their helpful comments and suggestions for improving the manuscript.

REFERENCES

1. J. R. Bates, *Semi-Lagrangian Advective Schemes and Their Use in Meteorological Modeling*, Lecture in Appl. Math., Vol. 22 (Am. Math. Soc., Providence, RI, (1985), p. 1.
2. R. Bermejo and A. Staniforth, *Mon. Weather Rev.* **120,** 2622 (1992).
3. A. Bott, *Mon. Weather Rev.* **117,** 1006 (1992).
4. J. R. Dougerthy, A. Edelman, and J. M. Hyman, *Math. Comput.* **52,** 471 (1989).
5. J. A. Edelman and C. A. Micchelli, *Numer. Math.* **51,** 441 (1987).
6. F. N. Fritsch and J. Butland, *SIAM J. Sci. Stat. Comput.* **5,** 300 (1984).
7. F. N. Fritsch and R. E. Carlson, *SIAM J. Numer. Anal.* **17,** 238 (1980).
8. P. Holnicki, *Mon. Weather Rev.* **123,** 862 (1995).
9. W. Hundsdorfer, B. Koren, M. van Loon, and J. G. Verwer, *J. Comput. Phys.* **117,** 35 (1995).
10. H. T. Huynh, *SIAM J. Numer. Anal.* **30,** 57 (1993).
11. A. Priestley, *Mon. Weather Rev.* **121,** 621 (1983).
12. M. Rančić, *Mon. Weather Rev.* **120,** 1394 (1992).
13. P. J. Rasch and D. L. Williamson, *SIAM J. Sci. Comput.* **11,** 656 (1990).
14. A. Staniforth and J. Côté, *Mon. Weather Rev.* **119,** 2206 (1991).
15. P. Smolarkiewicz and G. A. Grell, *J. Comput. Phys.* **101,** 431 (1992).
16. L. L. Takacs, *Mon. Weather Rev.* **113,** 1050 (1985).
17. D. L. Williamson and P. J. Rasch, *Mon. Weather Rev.* **117,** 102 (1989).